

Engineering excitonic metal-insulator transitions in ultra-thin doped copper sulfides

Haiyang Chen^{1*}, Yufeng Liu^{1*}, Yashi Jiang¹, Changcang Qiao¹, Tao Zhang¹, Jianyang Ding², Zhengtai Liu², Zhenhua Chen², Yaobo Huang², Jinfeng Jia^{1,3}, Shiyong Wang^{1,3#}, Peng Chen^{1#}

¹Tsung-Dao Lee Institute, Key Laboratory of Artificial Structures and Quantum Control (Ministry of Education), Shanghai Center for Complex Physics, School of Physics and Astronomy, Shanghai Jiao Tong University, Shanghai 200240, China.

²Shanghai Synchrotron Radiation Facility, Shanghai Advanced Research Institute, Chinese Academy of Sciences, 201204 Shanghai, China

³Hefei National Laboratory, Hefei 230088, China

*These authors contributed equally to this work.

#Email: shiyong.wang@sjtu.edu.cn;

pchen229@sjtu.edu.cn

Exciton condensation in the absence of optical excitation is proposed in 1960s to occur in a semiconductor at low temperatures when the binding energy of excitons overcomes the band gap or in a semimetal with weakly screened coulomb interaction, giving rise to an excitonic insulating state. However, it has been challenging to establish experimental realization in a natural material as the interacting electron-hole pockets rely on the band structures which are difficult to be delicately controlled. In this work, we demonstrate an excitonic insulating phase formed in ultra-thin copper sulfide films by effectively tuning the band structure via changing the composition of Cu and S in the system. Using angle-resolved photoemission spectroscopy (ARPES), we observed a continuous band renormalization and opening of a full gap at low temperatures over a wide range of doping. The electronic origin of the metal-insulator transition is supported by scanning tunneling microscopy (STM) and low energy electron diffraction (LEED) measurements, which show no indication of superlattice modulation and lattice symmetry breaking. The evidence of excitonic insulator is further provided by carrier density dependent transitions, a combined effect of electron screening and Coulomb interaction strength. Our findings demonstrate the tunability of the band structure of copper sulfides, allowing for new opportunities to study exotic quantum phases.

Many-body interactions hold significant importance in solids, allowing for the manifestation of collective excitations and macroscopic quantum phenomena [1–3]. One example is excitonic insulating phase originated from the coulomb interaction which gives rise to the spontaneous formation of bound electron-hole pairs [4–8]. Although success in realization of such a state in atomic double-layer system via electrically gating, conclusive evidence in a natural material remain challenging as considerable attention was paid to materials with interacting electron-hole pockets located at different momentums [9–17]. Condensation of excitons with finite-momentum will result in a charge density wave (CDW) which is difficult to distinguish from Peierls-type CDW induced by a lattice distortion. It is more promising to identify a condensed phase with zero-momentum excitons. However, exciton density deeply relies on the relative energies of electron and hole pockets. Methods of delicate control of the band structures thus become necessary.

Copper sulfides are a family of chemical compounds and minerals with the formula Cu_xS ($1 \leq x \leq 2$) [18–21]. They are intensively studied for the potential applications in thin-film solar cells and optoelectronics [22,23]. Although the long-standing interest in Cu_xS , its band structure has not been well revealed by experiments. Because of the structural complexity, Cu_xS has different phases. The stoichiometric compound CuS (covellite) is a *p*-type metal and Cu_2S (chalcocite) is a *p*-type semiconductor, in which the bulk band gap determined from optical absorption measurements is ~ 1.1 - 1.4 eV depending on the variation from the stoichiometric composition [20,24–28]. It is thus expected that the band gap of Cu_xS can be tuned via changing the composition of Cu/S in the system. This can be realized by annealing CuS films at high temperatures (220-450 °C) as CuS tends to decompose above 220 °C [29]. The loss of sulfur atoms will lead to a compositional change and form a series of Cu_xS with x in the range of [1, 2]. Furthermore, excitons have been shown around the onset of the band gap in Cu_xS [28,30], which

can result in an excitonic instability in the low temperatures when the gap becomes small, making Cu_xS an ideal platform for investigating the long-sought insulating state induced by spontaneous exciton condensation.

We start with growing ultrathin CuS films using molecular beam epitaxy (MBE) on a bilayer-graphene-terminated SiC substrate. ARPES spectra taken at 10 K show hole-like bands centered at the $\bar{\Gamma}$ point (Fig. S1), in consistent with the first-principles calculated results [20]. These bands cross over the Fermi level, indicating the system is metallic. Annealing of CuS film at different temperatures results in a varied composition of Cu and S, as manifested in different band structures observed by ARPES (Fig. S1). For example, annealing at 330 °C gives rise to a less *p* type doped system. More occupied valence bands below the Fermi level emerges compared with the CuS, as indicated in the ARPES spectra in Fig. 1(f) and Fig. S1. Sharp reflection high-energy electron diffraction (RHEED) patterns [Fig. 1(a)] reveal a high-quality and well-ordered film. Two hole-like bands around the $\bar{\Gamma}$ points are clearly observed in the ARPES spectra [Fig. 1(f)]. The β band is more prominent in the *s*-polarized spectra because of the matrix element effects, indicating Cu $3d_{xy}$ and S $3p_y$ orbitals dominate in this band [13,31].

Interestingly, a full gap opening around the $\bar{\Gamma}$ point is observed when the temperature is decreased to 10 K, demonstrating that the system becomes a semiconductor/insulator at low temperatures [Fig. 1(f)]. Strong band renormalization is observed as the flat band top is developed around the β band and the spectral intensity of the α band is suppressed near the Fermi level. Measurements with *p*-polarized light show a clearer α band (Fig. S3), demonstrating the two bands around the Fermi level have different orbital characters [32], which may explain their different behaviors in the low temperatures. The scanning tunneling microscopy (STM) measurements reveal Cu_xS islands with an uniform thickness distribution on top of graphene (Fig.

S2). A Fourier transform of the atomic topographic image [Fig. 1(c) and 1(d)] shows sharp (1×1) hexagonal lattice peaks and the in-plane lattice constant is determined to be ~ 4.0 Å, a lattice constant that is close to that of Cu_2S compared to the CuS compound (3.79 Å) [20,23,24]. Importantly, there is no superlattice modulation or translation symmetry breaking observed in the STM measurements.

To investigate the metal-insulator transition for the Cu_xS , we take systematic scans of the bands along $\overline{\Gamma\text{M}}$ [Fig. 2] as a function of temperature. Selected temperature-dependent s -polarized ARPES spectra for a Cu_xS sample are shown in Fig. 2(a). The gap formation is illustrated by the symmetrized ARPES maps in Fig. 2(b). The energy distribution curves (EDCs) around the zone center shown in Fig. 2(c) were symmetrized with respect to the Fermi level. By symmetrization, the effect of Fermi-Dirac distribution at high temperatures can be canceled out. A single peak at the Fermi level indicates the β band top crosses over the Fermi level at temperatures higher than 150 K. At lower temperatures, the observed two-peak structure indicates the opening of a gap around the Fermi level. The spectroscopic gap, determined from the difference between the β band top and the Fermi level, is ~ 80 meV at 10 K. The square of the energy gap as a function of temperature follows a functional form described by a semi-phenomenological mean-field equation [red solid curve in Fig. 2(f)] [33]. The fit yields a transition temperature of $T_C = 153 \pm 3$ K.

The above gap analysis is performed assuming the particle-hole symmetry in the system. We took STS scans to probe the density of states above the Fermi level. As shown in Fig. 3, STS results at 3.5 K reveal a small band gap ($2\Delta = 87$ meV) determined from the difference of the valence and conduction band energy for the interior of the Cu_xS islands (annealed at 320 °C), which is in excellent agreement with the ARPES result ($\Delta = 48$ meV). The density of states of conduction and valence bands are symmetric around the Fermi level, indicating the determination of the

spectroscopic gap is reasonable and suggesting the existence of electron-hole coherent interaction. A notable particle-hole asymmetry is presented in the samples without a phase transition, as shown in Fig. S7, in which more STS data and corresponding ARPES spectra for Cu_xS with different Cu/S ratio are included.

The *in-situ* LEED results on a Cu_xS film annealed at 330 °C ($T_C = 153$ K) are shown in Fig. 3(b). Clear diffraction spots with a hexagonal-shape (marked with red circles) from Cu_xS are observed at 10 K, which is in consistent with the structure determined by STM. The other set of weak diffraction spots marked with blue dashed circles are from the less preferred domains aligned with the underlying graphene. The rest spots are from the reconstructed $(6\sqrt{3} \times 6\sqrt{3})$ SiC surface and graphene [34,35]. The detailed assignments of the diffraction spots are shown in Fig. S8. Temperature dependent LEED data shows there are no significant changes associated with a structural transition, including emergence of new diffraction spots and notable shift of the spots across the transition. These measurements reveal the absence of any structural phase transition in the low temperatures. The observed band structure change by ARPES is purely electronic and in consistent with the excitonic insulator picture that the excitons condense at low temperatures, which minimizes the energy of Cu_xS system by opening a gap.

Annealing the CuS films at a higher temperature or with a longer time results in a similar band structure but a larger gap in ARPES measurements. To quantify the evolution of band structure with annealing temperatures, we extract the carrier density from the Luttinger area of the Fermi surface at 200 K in the normal phase [36]. The carrier density of the sample annealed at 330 °C is determined to be $1.4 \times 10^{13} \text{ cm}^{-2}$ (hole density p) around the zone center and the T_C is more than 3 times of the value from the films annealed at 320 °C with a carrier density of $3.8 \times 10^{13} \text{ cm}^{-2}$ ($T_C = 40$ K). However, annealing at higher temperatures causes a reduction of the T_C

and further annealing leads to a semiconductor/insulator in the normal phase, which shows a different band structure as α and β bands become fully occupied and merge at the $\bar{\Gamma}$ point (Fig. S1). There is no obvious band structure change with decreasing temperature to 10 K, indicating the system becomes a band insulator (Fig. S6).

The observed carrier density dependent behavior is consistent with the scenario of the excitonic insulator, a result from weakly screened Coulomb interaction in a semimetal. The summarized results are shown in a phase diagram [Fig. 4]. Annealing of thin CuS films has two effects on the band structure instead of a rigid shift of the chemical potential: less p -type carriers around the Fermi level caused by the loss of sulfur atoms and increase of the energy difference between valence and conduction bands. The former effect reduces the screening strength and benefits the formation of the excitons, as shown in the increased T_C for the samples with a hole density between 1.4 and $4.6 \times 10^{13} \text{ cm}^{-2}$. However, the latter effect gives rise to a weakened Coulomb interaction, which dominates for samples annealed at higher temperature than $330 \text{ }^\circ\text{C}$ and results in a smaller exciton density and a lower T_C .

In conclusion, copper sulfides over a wide range of doping provide a versatile platform to realize quantum states based on the interband electron-hole coherent interaction. Flexibility of the Cu/S composition and the corresponding tunability of the band structure is the key to make this system a unique case. The behavior of the metal-insulator transition with varied carrier densities is understood as a combined effect of electron screening and Coulomb interaction strength. Future study including terahertz spectroscopy with high vacuum is promising to unveil the low energy collective modes formed during the condensation for a complete understanding of the nature of the excitonic insulator [37].

Acknowledgments

We thank Shengwei Jiang, Jing Wang, Xiaoyan Xu, Mingpu Qing, Yanghao Chan for helpful discussions. The work at Shanghai Jiao Tong University is supported by the Ministry of Science and Technology of China under Grant No. 2022YFA1402400, No. 2021YFE0194100, No. 2020YFA0309000, the Science and Technology Commission of Shanghai Municipality under Grant No. 21JC1403000, the National Natural Science Foundation of China (Grant No. 12374188, No. 12488101, No. 22325203, No. 92265105). P. C. thanks the sponsorship from Yangyang Development Fund.

References

- [1] M. Imada, A. Fujimori, and Y. Tokura, Metal-insulator transitions, *Rev. Mod. Phys.* **70**, (1998).
- [2] J. Bardeen, L. N. Cooper, and J. R. Schrieffer, Theory of Superconductivity, *Phys. Rev.* **108**, 1175 (1957).
- [3] A. J. Leggett, Quantum Liquids, *Science* **319**, 1203 (2008).
- [4] N. F. Mott, The transition to the metallic state, *Philosophical Magazine* **6**, 287 (1961).
- [5] L. V. Keldysh and Yu. V. Kopayev, Possible Instability of the Semimetallic State toward Coulomb Interaction, *Sov. Phys. Solid State* **6**, 2219–2224 (1965).
- [6] D. Jérôme, T. M. Rice, and W. Kohn, Excitonic Insulator, *Phys. Rev.* **158**, 462 (1967).
- [7] B. I. Halperin and T. M. Rice, Possible Anomalies at a Semimetal-Semiconductor Transition, *Rev. Mod. Phys.* **40**, 755 (1968).
- [8] W. Kohn, Excitonic Phases, *Phys. Rev. Lett.* **19**, 439 (1967).
- [9] L. A. Jauregui *et al.*, Electrical control of interlayer exciton dynamics in atomically thin

- heterostructures, *Science* **366**, 870 (2019).
- [10] Z. Wang, D. A. Rhodes, K. Watanabe, T. Taniguchi, J. C. Hone, J. Shan, and K. F. Mak, Evidence of high-temperature exciton condensation in two-dimensional atomic double layers, *Nature* **574**, 76 (2019).
- [11] L. Ma, P. X. Nguyen, Z. Wang, Y. Zeng, K. Watanabe, T. Taniguchi, A. H. MacDonald, K. F. Mak, and J. Shan, Strongly correlated excitonic insulator in atomic double layers, *Nature* **598**, 585 (2021).
- [12] H. Yang, X. Wang, and X.-Z. Li, A scenario for high-temperature excitonic insulators, *New J. Phys.* **24**, 083010 (2022).
- [13] Q. Gao *et al.*, Evidence of high-temperature exciton condensation in a two-dimensional semimetal, *Nat Commun* **14**, 994 (2023).
- [14] Y. Song *et al.*, Signatures of the exciton gas phase and its condensation in monolayer 1T-ZrTe₂, *Nat Commun* **14**, 1116 (2023).
- [15] Q. Gao *et al.*, Observation of possible excitonic charge density waves and metal–insulator transitions in atomically thin semimetals, *Nat. Phys.* **20**, 597 (2024).
- [16] Y. Jia *et al.*, Evidence for a monolayer excitonic insulator, *Nat. Phys.* **18**, 87 (2022).
- [17] B. Sun *et al.*, Evidence for equilibrium exciton condensation in monolayer WTe₂, *Nat. Phys.* **18**, 94 (2022).
- [18] M. Posfai and P. R. Buseck, Djurleite, digenite, and chalcocite: Intergrowths and transformations, *American Mineralogist* **79**, 308 (1994).
- [19] D. J. Chakrabarti and D. E. Laughlin, The Cu-S (Copper-Sulfur) system, *Bulletin of Alloy Phase Diagrams* **4**, 254 (1983).
- [20] A. Morales-García, A. L. Soares, E. C. Dos Santos, H. A. De Abreu, and H. A. Duarte, First-

- Principles Calculations and Electron Density Topological Analysis of Covellite (CuS), *J. Phys. Chem. A* **118**, 5823 (2014).
- [21] H. T. Evans, Copper coordination in low chalcocite and djurleite and other copper-rich sulfides, *American Mineralogist* **66**, 807 (1981).
- [22] J. A. Bragagnolo, A. M. Barnett, J. E. Phillips, R. B. Hall, A. Rothwarf, and J. D. Meakin, The design and fabrication of thin-film CdS/Cu₂S cells of 9.15-percent conversion efficiency, *IEEE Trans. Electron Devices* **27**, 645 (1980).
- [23] W. Liu, L. Yang, Z. Chen, and J. Zou, Promising and Eco-Friendly Cu₂X-Based Thermoelectric Materials: Progress and Applications, *Advanced Materials* **32**, 1905703 (2020).
- [24] L.-W. Wang, High Chalcocite Cu₂S: A Solid-Liquid Hybrid Phase, *Phys. Rev. Lett.* **108**, 085703 (2012).
- [25] N. K. Abbas, and N. J. Ghdeeb, The effect of thickness on the optical properties of Cu₂S thin films, *Iraqi Journal of Physics* **13**, 121 (2019).
- [26] M. J. Buerger and B. J. Wuensch, Distribution of Atoms in High Chalcocite, Cu₂S, *Science* **141**, 276 (1963).
- [27] B. J. Mulder, Optical properties and energy band scheme of cuprous sulphides with ordered and disordered copper ions, *Phys. Stat. Sol. (a)* **18**, 633 (1973).
- [28] J. M. Luther, P. K. Jain, T. Ewers, and A. P. Alivisatos, Localized surface plasmon resonances arising from free carriers in doped quantum dots, *Nature Mater* **10**, 361 (2011).
- [29] M. T. S. Nair, L. Guerrero, and P. K. Nair, Conversion of chemically deposited CuS thin films to and by annealing, *Semicond. Sci. Technol.* **13**, 1164 (1998).
- [30] S. Couve, L. Gousskov, L. Szepessy, J. Vedel, and E. Castel, Resistivity and optical

- transmission of Cu_xS layers as a function of composition, *Thin Solid Films* **15**, 223 (1973).
- [31] N. Aryal and E. Manousakis, Importance of electron correlations in understanding photoelectron spectroscopy and Weyl character of MoTe_2 , *Phys. Rev. B* **99**, 035123 (2019).
- [32] P. Lukashev, W. R. L. Lambrecht, T. Kotani, and M. Van Schilfgaarde, Electronic and crystal structure of Cu_{2-x}S : Full-potential electronic structure calculations, *Phys. Rev. B* **76**, 195202 (2007).
- [33] M. R. Norman, M. Randeria, H. Ding, and J. C. Campuzano, Phenomenology of the low-energy spectral function in high- T_c superconductors, *Phys. Rev. B* **57**, R11093 (1998).
- [34] P. J. Fisher, Luxmi, N. Srivastava, S. Nie, and R. M. Feenstra, Thickness monitoring of graphene on SiC using low-energy electron diffraction, *Journal of Vacuum Science & Technology A: Vacuum, Surfaces, and Films* **28**, 958 (2010).
- [35] G. Yazdi, T. Iakimov, and R. Yakimova, Epitaxial Graphene on SiC: A Review of Growth and Characterization, *Crystals* **6**, 53 (2016).
- [36] H.-B. Yang, *et al*, Fermi Surface Evolution and Luttinger Theorem in Na_xCoO_2 : A Systematic Photoemission Study, *Phys. Rev. Lett.* **95**, 146401 (2005).
- [37] Y. Murakami, D. Golež, T. Kaneko, A. Koga, A. J. Millis, and P. Werner, Collective modes in excitonic insulators: Effects of electron-phonon coupling and signatures in the optical response, *Phys. Rev. B* **101**, 195118 (2020).

FIG. 1 Film structure and electronic band structure of ultra-thin Cu_xS . (a) A RHEED pattern of thin Cu_xS film taken at room temperature. (b) Core-level photoemission spectra taken with 110 eV photons. (c) An atomic topographic image of Cu_xS film. ($V_{\text{Bias}} = -1.5$ V; $I_t = 100$ pA). (d) A pattern derived from the Fourier transform of the image. (e) Schematic diagram for evolution of the band structure and the opening of a gap around the Fermi level originated from the exciton condensation when decreasing temperature. (f) ARPES maps taken with s polarized light for Cu_xS in the normal phase at 200 K and in the condensed phase at 10 K.

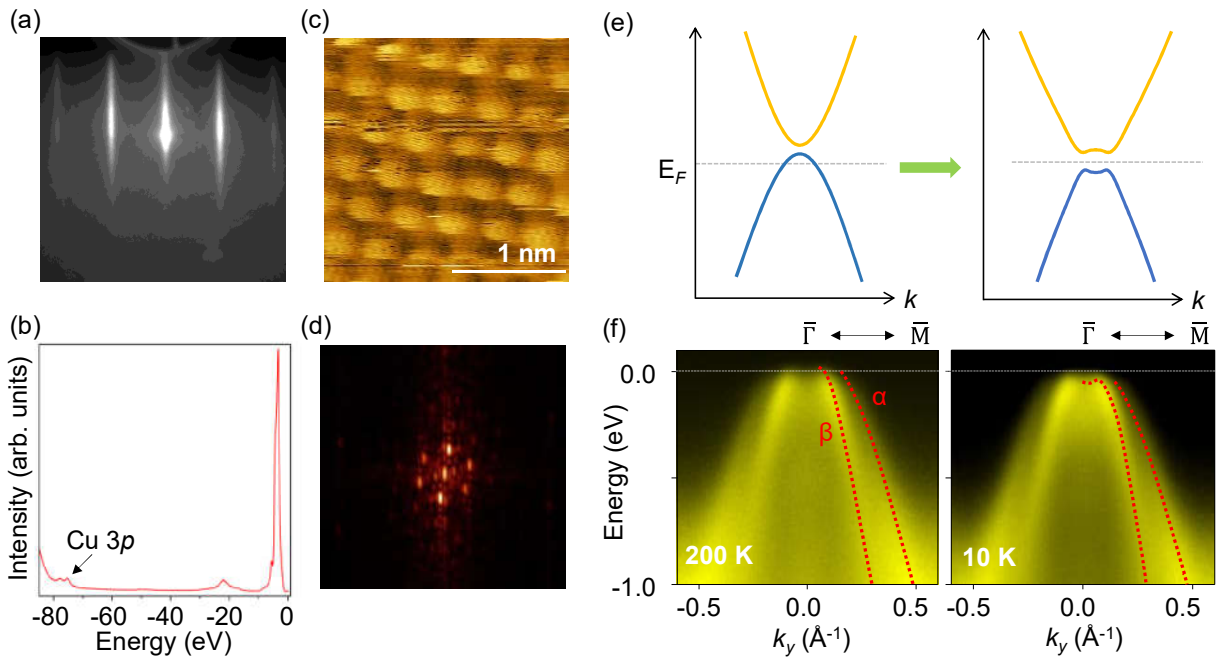


FIG. 2 Temperature dependence of the band structure and the energy gap. (a) ARPES spectra reveal the development of the flat top of β band when the temperature is decreased from 200 to 10 K. The data were taken with 28 eV *s*-polarized photons. The red arrow indicates the momentum position that the β band crosses the Fermi level. (b) Corresponding symmetrized ARPES maps show the evolution of the gap around the zone center with temperature. (c) EDCs around the zone center indicated by the red arrow in (a) at selected temperatures, the leading-edge midpoints are demonstrated by a black arrow. (d) Symmetrized EDCs at the zone center at selected temperatures between 10 and 300 K. By symmetrization, the effect of Fermi-Dirac distribution at high temperatures can be canceled out. (e) The extracted temperature dependence of the square of the energy gap. The red curve is a fit using a BCS-type mean-field equation. Transition temperature T_C is labeled.

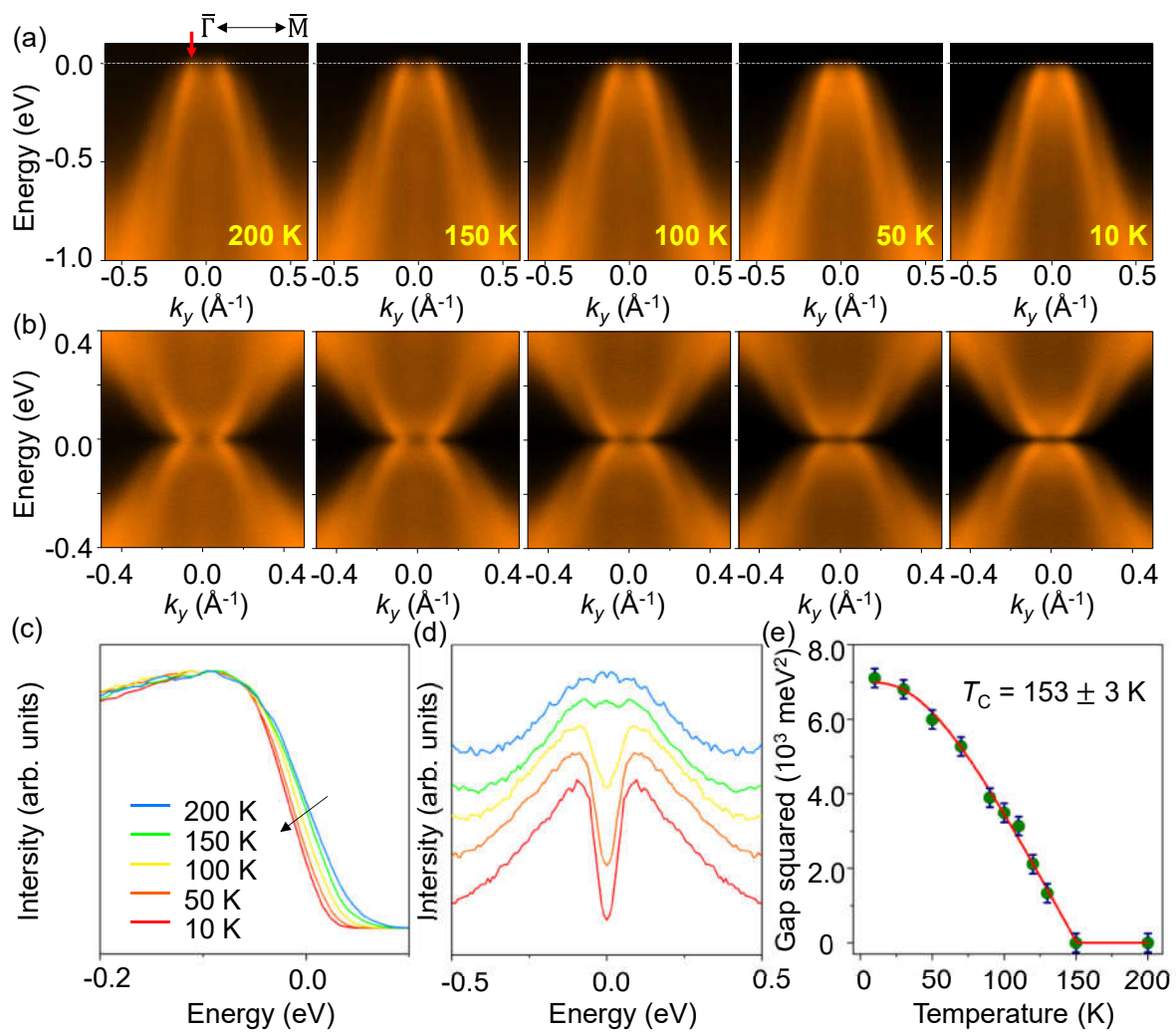


FIG. 3 The tunneling spectral gaps and temperature dependent LEED patterns for Cu_xS films. (a) dI/dV spectra taken at the interior of the Cu_xS islands at 3.5 K are superimposed on top of the ARPES spectra taken along the $\bar{\Gamma}\bar{M}$ direction. The arrows indicate the valence and conduction band positions. Below the Fermi level, the valence band position matches well with the ARPES data. (b) Evolution of Cu_xS (annealed at 330 °C) diffraction spots with decreasing temperature. Two preferred orientations of Cu_xS domains are revealed and no notable changes are observed across the transition.

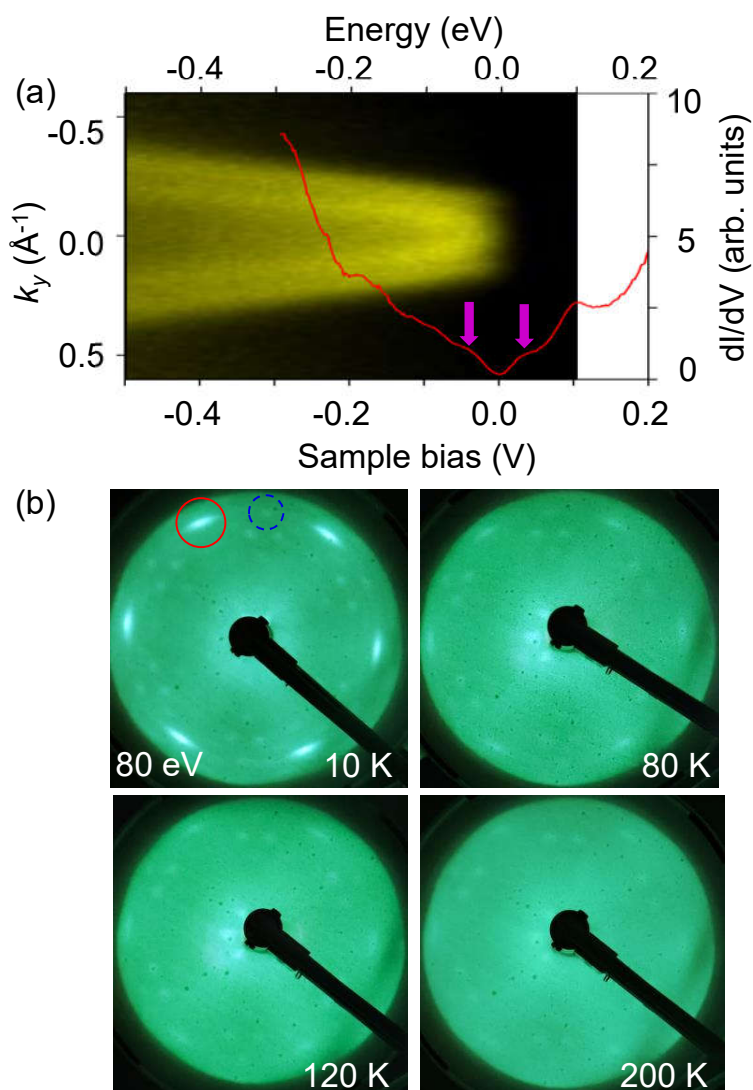


FIG. 4 Phase diagram for Cu_xS . Transition temperature as a function of hole carrier density (p) around the Fermi level. Schematic diagrams of the electronic structure for different carrier densities are shown to demonstrate the relation of the band structure of Cu_xS with the phase transition. The grey dashed line in each diagram denotes the Fermi level.

